Confinement of vacancies during annealing of H implanted GaN sandwiched between two InGaN/GaN superlattices

Nikolay Cherkashin, Alain Claverie, D. Sotta, J.-M. Bethoux, L. Capello, O. Kononchuk

Confinement of vacancies during annealing of H implanted GaN sandwiched between two {InGaN/GaN} superlattices

N. Cherkashin, A. Claverie, D. Sotta, J.-M. Bethoux, L. Capello, and O. Kononchuk

Citation: Appl. Phys. Lett. **101**, 023105 (2012); doi: 10.1063/1.4733619
View online: https://doi.org/10.1063/1.4733619
View Table of Contents: http://aip.scitation.org/toc/apl/101/2
Published by the American Institute of Physics

Confinement of vacancies during annealing of H implanted GaN sandwiched between two {InGaN/GaN} superlattices

N. Cherkashin,[1,a)] A. Claverie,[1] D. Sotta,[2] J.-M. Bethoux,[2] L. Capello,[2] and O. Kononchuk[2]
[1]*CEMES, CNRS UPR 8011 et Université de Toulouse, 29 rue Jeanne Marvig, 31055 Toulouse, France*
[2]*SOITEC S.A., Core Technologies R&D, Parc Technologique des Fontaines, 38190 Bernin, France*

(Received 16 April 2012; accepted 19 June 2012; published online 9 July 2012)

Using transmission electron microscopy techniques, we identify the extended defects of interstitial and vacancy types found after H implantation and annealing in GaN. We statistically analyze the effect of boarding or sandwiching GaN between strained superlattices on these populations of defects. We finally demonstrate the possibility to use compressively strained layers to localize and favour the precipitation of vacancy type defects in GaN. The source of excess vacancies, the mechanism responsible for the cavity localization, and the drastic increase of their volume fraction are discussed. © *2012 American Institute of Physics*. [http://dx.doi.org/10.1063/1.4733619]

H^+ ion implantation followed by annealing can be used to transfer high quality single crystalline GaN layers onto sapphire wafers using the Smart Cut™ technology.[1] However, for still unclear reasons, the H^+ fluences necessary to obtain full splitting of GaN layers are about one order of magnitude higher than those typically used for transferring other semiconductor materials such as Si, Ge, GaAs, InP, and SiC.[2] In the SmartCut™, hydrogen ion implantation followed by wafer bonding and thermal annealing results in the precipitation of hydrogen and vacancies during annealing in the form of quasi-two dimensional defects filled with overpressurized H_2 gas and named platelets. Further annealing leads to their transformation into nano- and microcracks and, eventually, to the complete exfoliation of the upper layer.[3] No additional defects such as dislocations or clusters of interstitials have been detected in these materials so far. On the contrary, H^+ implantation in GaN followed by annealing results in the formation of high densities of stacking faults (SFs), pyramidal voids, and nano-bubbles.[4–6] The presence of platelets was reported only after relatively low temperature annealing.[4,7] While the platelets formed in Si look like homogeneous disks, platelets in GaN are apparently formed by the planar agglomeration of nano-bubbles. Thus, the considerable difference in the minimal H fluences necessary for the exfoliation of GaN and Si should be related to the difference in the types of defects formed in both matrices after H implantation and annealing.[6]

The preferential nucleation and favoured growth of platelets at or close to strained layers has been previously observed in Si and SiGe.[8–10] Both (in plane) compressively and tensely strained layers act as effective traps for H atoms during annealing, although the driving forces might be different.[9,10] However, keeping in mind the difference in the types of defects formed in Si and GaN crystals after H implantation and annealing, the effect of strained layers on the H/vacancy precipitation in GaN is not obvious and merits an independent investigation.

In this work, we investigate the effect of strained layers on the H/vacancy precipitation by using adequate quantitative transmission electron microscopy (TEM) techniques. First, we identify the extended defects of interstitial and vacancy types found in the implanted zone after H^+ implantation into GaN and annealing. Then, we study the effect of sandwiching the GaN region to be implanted between metamorphic (in-plane), either compressively or tensely strained {InGaN/GaN} and {AlGaN/GaN}, superlattices (SLs), respectively, onto the populations of defects. We evidence that the {InGaN/GaN} SLs are extremely efficient to confine and favour vacancy precipitation. In contrast, the tensely strained {AlGaN/GaN} SLs have little effect.

All the samples were grown by metalorganic chemical vapor deposition (MOCVD) on (0001) sapphire substrates using the standard 2-steps buffer layer technique.[11] First, two reference samples of about 4 μm-thick Ga-terminated GaN layers were implanted by H^+ ions at 60 keV with a fluence of 2×10^{17} cm^{-2} (further on referenced as the "high fluence") or 0.5×10^{17} cm^{-2} (further on referenced as the "low fluence"). Analysis of the H depth distributions by secondary ion mass spectroscopy (SIMS) shows that the maximum H concentration is reached at a depth of 420–450 nm from the surface (as schematized in Fig. 1(a)). Three structures containing SLs, either $10 \times$ {3 nm-thick $In_{0.15}Ga_{0.85}N$/3 nm-thick GaN} (further on referenced as the InGaN SLs) or $10 \times$ {3 nm-thick $Al_{0.15}Ga_{0.85}N$/3 nm-thick GaN} (further on referenced as the AlGaN SLs) were grown with characteristics as shown in Figs. 1(b)–1(d). These structures were implanted by H^+ ions at 60 keV with the high fluence. Note that, in all cases, the SLs border or surround the implanted zone. The composition and the thickness of the layers composing the SLs were verified by x-ray diffraction. All layers are fully strained on the GaN crystal, and the threading dislocation density is in the $(1–3) \times 10^8$ cm^{-2} range. Further on, these three structures and the reference sample were annealed at 700 °C during 10 min. Specimens from all these samples were prepared for cross-sectional (X) imaging along ⟨2-1-10⟩ and ⟨10-10⟩ directions by tripod polishing and low energy/current density argon ion-beam thinning until electron transparency. High-resolution TEM (HRTEM) imaging was performed on the SACTEM-Toulouse, a Tecnai F20 (FEI) operating at 200 kV equipped with an imaging aberration corrector (CEOS). "Conventional" diffraction contrast

[a)]Author to whom correspondence should be addressed. Electronic mail: nikolay.cherkashin@cemes.fr.

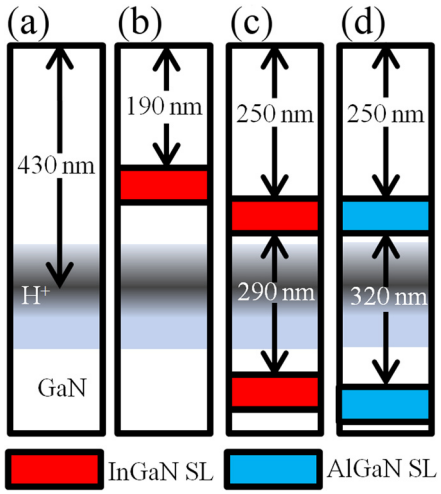

FIG. 1. Schematic representation of the different samples: reference sample (a), GaN boarded by one InGaN SL (b), GaN sandwiched by 2 InGaN SLs (c), and GaN sandwiched by 2 AlGaN SLs (d).

imaging was performed on a Jeol 2010 TEM operating at 200 kV.

We have analysed the structure of the extended defects formed after low fluence implantation and annealing in the GaN reference sample using appropriate diffraction conditions. Fig. 2(a) is a dark-field image taken close to the $[2\bar{1}\bar{1}0]$ zone axis with $g = 01\bar{1}0$ and under exact two-beam conditions. Sharp black lines on a white background are seen lying perpendicular to the [0001] direction. With $g = 0002$, this contrast disappears and is replaced by a strong diffraction contrast surrounding the same regions (Fig. 2(b)). The HRTEM image of one of these defects (Fig. 2(c)) evidences one additional (0002) plane, *C*, built of both Ga and N atoms. This additional plane locally creates a SF showing the sequence AB***C***AB. The combination of all these characteristics proves that these objects are Frank dislocation loops (DLs) lying on the basal (0001) plane with a Burgers vector $b = 1/2[0001]$. Such extrinsic prismatic Frank DLs can be formed only by the precipitation, during annealing, of "excess" Ga and N atoms initially on interstitial sites. Actually, these defects are by far the predominant defects seen in these GaN layers, whatever the dose, low or high.

We have statistically analysed these DL populations over several images and measured their size distributions, their surface densities, and the integrated number of interstitials they contain. The thickness of the TEM lamella in a given area was estimated using extinction fringes obtained for $g = 0002$. Details of the measurement technique of DLs and vacancy clusters could be found in our previous works.[3,10,12]

We find that the average length of the side of the hexagonal base of the DLs is independent of the implanted fluence and equals to 6.5 ± 0.5 nm. However, the density of DLs (projected over the 250–300 nm-thick defective band) is apparently proportional to the implanted fluence since it equals $(0.5–0.7) \times 10^{13}\,\mathrm{cm}^{-2}$ and $(1–4) \times 10^{13}\,\mathrm{cm}^{-2}$ for the low and high fluences, respectively. From these data, one obtains the number of Ga and N atoms contained within the DL populations, N_{proj}^{int}, equals to $(0.2–0.4) \times 10^{17}\,\mathrm{atom/cm}^2$ and to $(0.8–3) \times 10^{17}\,\mathrm{atom/cm}^2$ for the low and high fluences, respectively. This proportionality between the fluence and the number of atoms stored within the defects confirms the "precipitate" nature of the extrinsic or Frank DLs.[15]

The interstitial atoms which precipitate within DLs must be those, initially created by the displacement cascades induced by H implantation, which survive recombination with their vacancy counterparts and possible exodiffusion at the wafer surface during implantation and annealing. Thus, roughly the same number of vacancies had to exist in some form in the damage zone.

Indeed, vacancy type defects are detected in this region. They are clearly seen in images taken under bright field and underfocused conditions, with $g = 0008$ (Fig. 2(d)). This type of contrast (see inset in Fig. 2(d)) and the systematic orientation of their triangular shape suggest that these defects

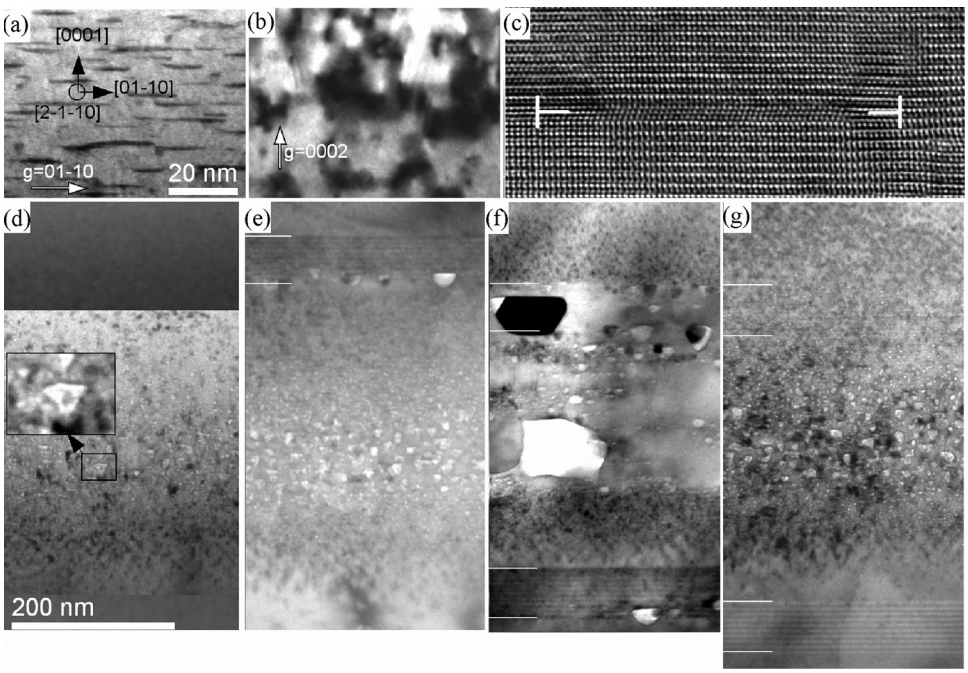

FIG. 2. Dark-field cross-section $(2\bar{1}\bar{1}0)$ images of the reference GaN sample taken with $g = 01\bar{1}0$ (a) and with $g = 0002$ (b), and HRTEM image of one Frank DL (c). Bright-field underfocused cross-section $(2\bar{1}\bar{1}0)$ images taken with $g = 0008$ of the reference sample (d), containing one InGaN SL (e), two InGaN SLs (f), and two AlGaN SLs (g). All samples have been implanted with the high fluence and annealed at 700 °C for 10 min.

are empty (or H gas filled) pyramids with the N-terminated base parallel to the (0001) plane, 6 N-terminated $\{01\bar{1}\bar{1}\}$ sides, and the base- apex vector along the downward $[000\bar{1}]$ direction, as also observed in Ref. 6. The presence of only N-terminated sides to form these pyramids proves that their internal surfaces are passivated by H atoms, since Ga does not make stable bond with H.

We have also analysed these pyramids over several images to measure their size depth-distributions, their concentration, and volume fraction. The depth position of a pyramid is taken equal to that of its base. The "size" of a pyramid is defined by the length of its base which is 1.73 times smaller than the length of the base of a triangle obtained by projecting the pyramid along the $[2\bar{1}\bar{1}0]$ direction.

Figs. 3(a), 3(d), and 3(g) show that the pyramids are well-distributed within the same 300 nm-thick damage zone than the DLs. Their size distribution is symmetrical with a sharp peak value of about 6 nm in the middle of the damage zone. The concentration of cavities has a local minimum at the same depth, and it increases before vanishing when moving towards the surface and the depth of the substrate (Fig. 3(d)). The volume fraction mimics the size distribution with larger shoulders on both sides of the maximum due to the large concentration of small pyramids found in these regions (Fig. 3(g)). These data are characteristics of the growth of a population of precipitates obtained by annealing of "impurities" implanted with high doses, i.e., where their growth rate depends on the initial supersaturation.[13–15]

However, from these measurements, the number of vacancies, N_{proj}^{vac}, contained within the pyramids can be calculated as $N_{proj}^{vac} = t\sum_{depth} V^{cav} c^{cav} c^{Ga@N}$, where V^{cav} is the average volume of the pyramids located at a given depth, c^{cav} is the concentration of pyramids at the same depth, and $c^{Ga@N} = 8.98 \times 10^{22}\,\mathrm{cm}^{-3}$ is the atomic density of GaN. From Fig. 3(g), one obtains N_{proj}^{vac} equal to $(0.05–0.07) \times 10^{17}$ atom/cm^2. This number is 70 times smaller than the number of interstitials found in the DLs after the same implantation. Thus, this imbalance suggests that either most vacancies have annihilated at the surface during annealing or that they are present in the form of point defects or small complexes not detected by TEM.

Figs. 2(e)–2(g) are images of the structures containing one upper InGaN SL, two InGaN SLs, and two AlGaN SLs, respectively, all implanted with the high fluence and annealed. These images are aligned using the wafer surface,

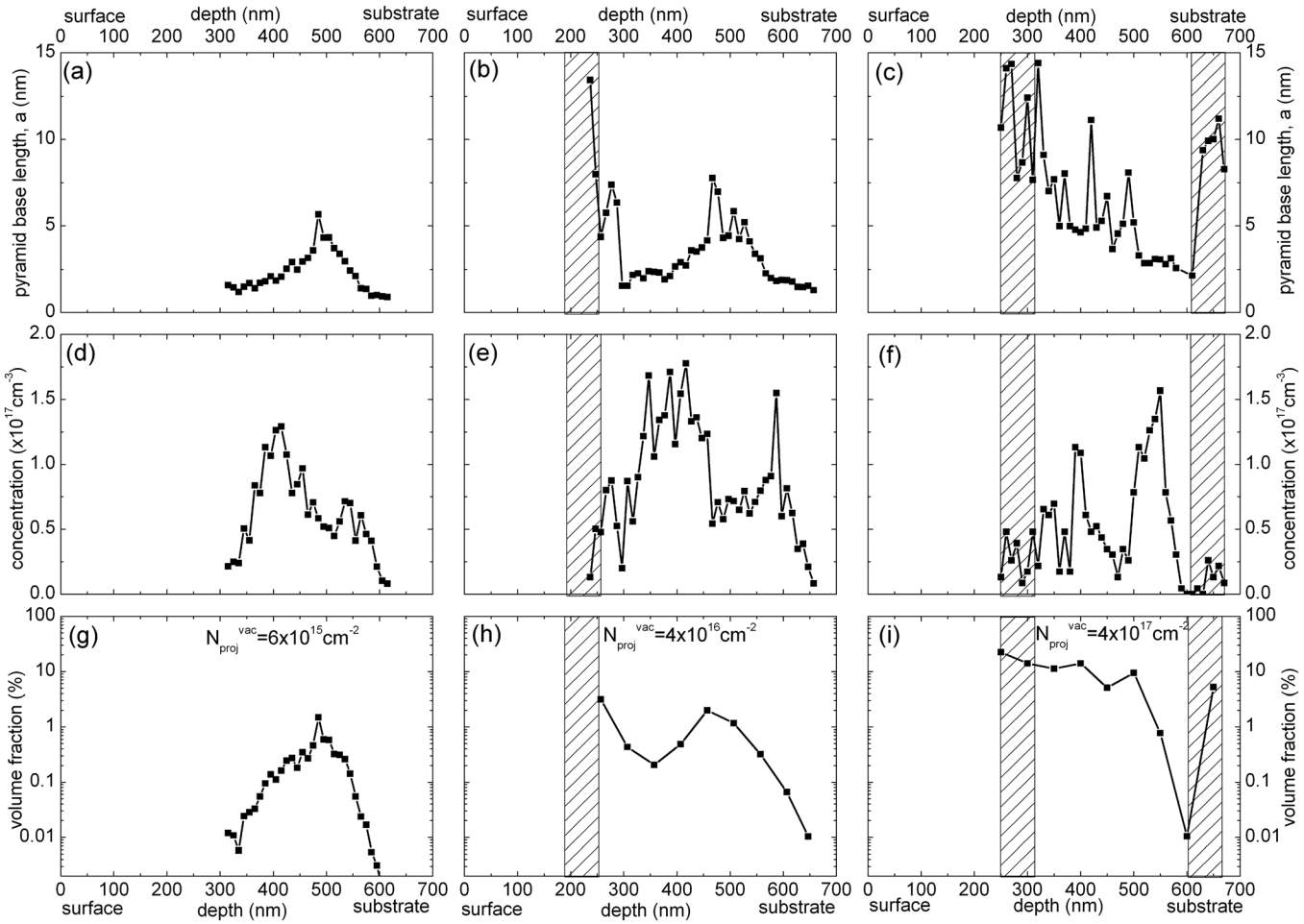

FIG. 3. Depth-distributions of mean sizes of pyramids in the reference sample (a), in the sample containing one InGaN SL (b), and in the sample containing two InGaN SLs (c). Depth-distributions of concentrations in the reference sample (d), in the sample containing one InGaN SL (e), and in the sample containing two InGaN SLs (f). Volume fraction occupied by the pyramids and cavities in the reference sample (g), in the sample containing one InGaN SL (h), and in the sample containing two InGaN SLs (i). Results compiled for "depth-classes" of 10 nm wide for the sizes and the concentrations and of 50 nm for the volume fraction. The relative uncertainties in these measurements are 5%, 20%, and 40%, respectively. The "size" of a pyramid is defined by the length of its base.

not seen in the print of Fig. 2. The upper/bottom boundaries of the SLs are delineated by white lines.

Qualitatively, all structures contain similar defects, DLs and pyramids. In the following, we focus on the different populations of pyramids found in these layers. First, we note that the presence of the two AlGaN SLs (Fig. 2(g)) has no effect on the pyramid population: they have similar size and concentration depth-distributions as in the reference sample. By contrast, pyramids and facetted cavities are found within the InGaN SLs (Figs. 2(e) and 2(f)), sometimes with sizes considerably larger than in the central GaN region, and thus at depths where none were found in the reference sample. It is to note that the image of the upper InGaN layers is blurred, the SLs are almost invisible, while some large pyramids and polyhedra show a strong dark contrast. This suggests that some transfer of In from the SLs towards large pyramids has taken place during annealing.

As evidenced in Figs. 3(b), 3(e), and 3(h), the presence of one upper InGaN SL does not affect neither the shape of the distributions nor the depth range over which the pyramids are distributed in the GaN crystal. "Additional" cavities appear close to and at the bottom layers of the InGaN SL. Their size and the volume fraction they occupy are more than twice larger than the maximum values reached in the reference sample. The number of vacancies N_{proj}^{vac} stored by all these defects is $(0.3–0.5) \times 10^{17}$ atom/cm^{-2}, one order of magnitude larger than in the reference sample.

In the structure with two InGaN SLs, the cavities are distributed within the whole 450 nm-thick band including the SLs (Figs. 3(g)–3(i)). The size depth-distribution shows three peaks: (1) at the upper InGaN SL, (2) at the projected range of the ions, as in the reference sample, and (3) at the deeper InGaN SL. The largest cavities are found in the top SL and in the deeper one where their density is smaller. In the GaN crystal sandwiched by the two SLs, the pyramids are significantly larger than in the reference sample but also larger than in the structure containing only one SL. Their concentration depth-profile shows the overall shape already evidenced in the reference sample but with larger amplitude and increased contribution from the deeper part of GaN, close to the SL. The volume fraction occupied by the pyramids/cavities is maximum at about 20% at the top InGaN SL then it smoothly decreases from 15% to 10% within GaN as the depth increases and suddenly drops down to almost 0 near the deep SL. This time, the number of vacancies stored by all these defects, N_{proj}^{vac}, is $(2–5) \times 10^{17}$ atom/cm^2, two orders of magnitude higher than in the reference sample, and very close to the number of interstitials found in the same region, N_{proj}^{int}.

Our results show the dramatic effect of sandwiching GaN between two compressively strained InGaN layers. Two characteristics are of main interest: (i) amplitude—the volume fraction occupied by the pyramids increases by a factor of 100 when sandwiching and (ii) position—the pyramids are significantly larger within or at the interfaces of the SLs than in the implanted GaN.

Point (i) obviously demonstrates that the InGaN SLs and the defects which are attached to them prevent the massive exodiffusion of vacancies out of the GaN implanted region during annealing. Point (ii) demonstrates the massive transfer of vacancies which has taken place between the implanted region and the SLs.

These two characteristics suggest a possible scenario to describe the precipitation during annealing of vacancies in GaN sandwiched between two InGaN SLs.

At the very beginning of the annealing, vacancies partly interact to precipitate in the implanted region and partly diffuse out driven by the large concentration gradients on both sides of the implanted profile. As soon as vacancies reach the InGaN layers, they agglomerate as clusters or small cavities. It is easier to form small stable vacancy clusters, in other words the nucleation barrier is smaller, in or close to a compressively strained layer than in GaN matrix, since these defects, themselves, induce tensile stress in their surroundings, therefore, relaxing the overall stress in the system.[9,10,16] Thus, stable vacancy clusters form sooner at the SLs than in the GaN. During their nucleation, the supersaturation of (free) vacancies suddenly drops down to the (small) value imposed by the thermodynamical equilibrium with the cavities.[13] The resulting large concentration gradient between the implanted region and these cavities further drives more vacancies towards them, accelerating their growth. Later on, when nucleation in GaN is complete and that the cavities grow locally by Ostwald ripening, they are smaller than those located in the SLs. Consequently, although smaller, a concentration gradient always exists between the pyramids/cavities located in GaN and at the SLs and continuously drives the vacancies from one region to the others. It is to note that the dramatic reduction of vacancy exodiffusion from the implanted region is not due to the fact that SLs act as diffusion barriers for vacancies. Actually, the presence of cavities and pyramids weakens the concentration gradients driving the vacancies out of the implanted region. Moreover, as evidenced by our quantitative data, most if not all the vacancies reaching the SLs regions get trapped by the cavities and pyramids.

In summary, we have studied by TEM the effect of sandwiching GaN between two compressively strained InGaN or tensely strained AlGaN SLs onto the precipitation and growth of the extended defects formed by H implantation and annealing. Interstitials precipitate as Frank DLs while vacancies mostly precipitate in the form of pyramids whose internal surfaces are passivated by H atoms. In pure GaN, vacancies massively diffuse out of the implanted region indicating that the nucleation barrier to form stable, immobile, vacancy clusters is relatively large. Boarding GaN on one side or sandwiching it on both sides with tensely strained AlGaN SLs has no effect on these precipitation phenomena. In contrast, using compressively strained InGaN SLs, vacancy out diffusion can be inhibited and this phenomenon can be explained by logically assuming, based on stress arguments, that the nucleation barrier for cavity formation is smaller in or close to the InGaN SLs than in GaN. Further clarification of the efficiency of the compressively strained layers to capture vacancies in GaN needs some additional investigations based on an isochronal and an isothermal annealing, variations in H/vacancy concentration gradients (by coupling an amplitude of a H fluence/distance between {InGaN/GaAs} SLs), and in the stress/strain in InGaN layers. However, it is the presence of pyramids and cavities of larger sizes in or close to the InGaN SLs than in GaN, and not an intrinsic characteristic of these SLs, which prevents vacancies to diffuse out from the region.

Finally, this study points out the possibility to confine vacancies, and probably H implanted atoms, within a thin slice of GaN and to transform the latter into a highly porous layer if implanted with a high H fluence and annealed at a sufficiently high temperature. Our experimental findings allow to explain the possible origin of rather high H fluence required for exfoliation of GaN layers by outdiffusion of vacancies due to significant nucleation barrier for their precipitation.

[1]A. Tauzin, T. Akatsu, M. Rabarot, J. Dechamp, M. Zussy, H. Moriceau, J. F. Michaud, A. M. Charvet, L. Di Cioccio, F. Fournel, J. Garrione, B. Faure, F. Letertre, and N. Kernevez, Electron. Lett. **41**(11), 668 (2005).
[2]R. Singh, S. H. Christiansen, O. Moutanabbir, and U. Gösele, J. Electron. Mater. **39**(10), 2177 (2010).
[3]S. Personnic, F. Letertre, A. Tauzin, N. Cherkashin, A. Claverie, R. Fortunier, and H. Klocker, J. Appl. Phys. **103**(1), 023508 (2008).
[4]I. Radu, R. Singh, R. Scholz, U. Gösele, S. Christiansen, G. Brüderl, C. Eichler, and V. Härle, Appl. Phys. Lett. **89**, 031912 (2006).
[5]O. Moutanabbir, R. Scholz, S. Senz, U. Gösele, M. Chicoine, F. Schiettekatte, F. Süßkraut, and R. Krause-Rehberg, Appl. Phys. Lett. **93**, 031916 (2008).
[6]C. H. Seager, S. M. Myers, G. A. Petersen, J. Han, and T. Headley, J. Appl. Phys. **85**(5), 2568 (1999).
[7]O. Moutanabbir, R. Scholz, U. Gösele, A. Guittoum, M. Jungmann, M. Butterling, R. Krause-Rehberg, W. Anwand, W. Egger, and P. Sperr, Phys. Rev. B **81**, 115205 (2010).
[8]L. Shao, Y. Lin, J. G. Swadener, J. K. Lee, Q. X. Jia, Y. Q. Wang, M. Nastasi, P. E. Thompson, N. D. Theodore, P. K. Chu, T. L. Alford, J. W. Mayer, P. Chen, and S. S. Lau, Appl. Phys. Lett. **87**, 091902 (2005).
[9]A. J. Pitera and E. A. Fitzgerald, J. Appl. Phys. **97**, 104511 (2005).
[10]F. Okba, N. Cherkashin, Z. Di, M. Nastasi, F. Rossi, A. Merabet, and A. Claverie, Appl. Phys. Lett. **97**, 031917 (2010).
[11]S. Nakamura and G. Fasol, *The Blue Laser Diode* (Springer-Verlag, Berlin, 1997).
[12]J. Grisolia, G. Ben Assayag, and A. Claverie, Appl. Phys. Lett. **76**, 852 (2000).
[13]P. W. Voorhees, Annu. Rev. Mater. Sci. **22**, 197–215 (1992).
[14]N. A. Bert, A. I. Veinger, M. D. Vilisova, S. I. Goloshchapov, I. V. Ivonin, S. V. Kozyrev, A. E. Kunitsyn, L. G. Lavrentyeva, D. I. Lubyshev, V. V. Preobrazhenskii, B. R. Semyagin, V. V. Tretyakov, V. V. Chaldyshev, and M. P. Yakubenya, Phys. Solid State **35**(10), 1289 (1993).
[15]N. A. Cherkashin, A. Claverie, C. Bonafos, V. V. Chaldyshev, N. A. Bert, V. V. Preobrazhenskii, M. A. Putyato, B. R. Semyagin, and P. Werner, J. Appl. Phys. **102**, 023520 (2007).
[16]M. Nastasi, T. Höchbauer, J. K. Lee, A. Misra, J. P. Hirth, M. Ridgway, and T. Lafford, Appl. Phys. Lett. **86**, 154102 (2005).